International Journal of Mass Spectrometry 277 (2008) 113–122

Contents lists available at ScienceDirect

International Journal of Mass Spectrometry

journal homepage: www.elsevier.com/locate/ijms

Highly resolved absolute cross-sections for dissociative electron attachment to SF_5CF_3

K. Graupner[a], L.M. Graham[a], T.A. Field[a], C.A. Mayhew[b], I.I. Fabrikant[c], T.M. Miller[d], M. Braun[e], M.-W. Ruf[e], H. Hotop[e,*]

[a] Department of Physics and Astronomy, Queen's University, Belfast BT7 1NN, UK
[b] School of Physics and Astronomy, University of Birmingham, Birmingham B15 2TT, UK
[c] Department of Physics and Astronomy, University of Nebraska, Lincoln, NE 68588-0111, USA
[d] Air Force Research Laboratory, Hanscom Air Force Base, Bedford, MA 01731-3010, USA
[e] Fachbereich Physik, Technische Universität Kaiserslautern, D-67653 Kaiserslautern, Germany

ARTICLE INFO

Article history:
Received 31 March 2008
Received in revised form 14 May 2008
Accepted 19 May 2008
Available online 27 May 2008

Keywords:
Electron attachment
Cross-section
Branching ratio
R-matrix calculation
SF_5CF_3

ABSTRACT

Using two complementary experimental methods, we have measured partial (mass-resolved) cross-sections for dissociative electron attachment to the molecule trifluoromethyl sulfurpentafluoride (SF_5CF_3) at the gas temperature $T_G = 300$ K over a broad range of electron energies ($E = 0.001$–12 eV). The absolute scale for these cross-sections was obtained with reference to the thermal ($T = 300$ K) rate coefficient for anion formation ($8.0(3) \times 10^{-8}$ cm^3 s^{-1}). Below 1 eV, SF_5^- is the dominant product anion and formed through the lowest anion state which cuts the neutral SF_5CF_3 potential close to the S–C equilibrium distance. The highly resolved laser photoelectron attachment data exhibit a downward Wigner cusp at 86 meV, indicating that the $\nu_4(a_1)$ vibrational mode is important for the primary attachment dynamics. Both SF_5^- and F^- anions are formed with similar yields through the first excited resonance located near 3.6 eV. Towards higher energies, the anions CF_3^-, SF_4^-, and SF_3^- are also produced. Summation of the partial cross-sections yields a total absolute cross-section for anion formation over the energy range 0.001–12 eV. This is used to calculate the dependence of the rate coefficient for dissociative electron attachment over a broad range of electron temperatures for the fixed gas temperature $T_G = 300$ K; good agreement is found between the calculated values and those obtained in a drift tube experiment. In addition to the experimental work, semiempirical R-matrix calculations have been carried out for the energy dependence of the cross-section for SF_5^- formation. The experimental findings are semi-quantitatively recovered.

1. Introduction

An analysis of stratospheric air samples by Sturges et al. [1] has indicated that trifluoromethyl sulfurpentafluoride (SF_5CF_3) is present in the stratosphere. The compound is thought to be exclusively anthropogenic in origin; it has been speculated that the source of atmospheric SF_5CF_3 may be the reaction of SF_6 with fluoropolymers in electrical devices (see papers by Huang et al. [2] and by Tsai [3,4]). Although present at a level of only 0.12 ppt in 1999, the atmospheric abundance of SF_5CF_3 is reportedly increasing by 6% per year, tracking the increase of atmospheric SF_6 [1]. This is significant because both SF_6 and SF_5CF_3 are powerful greenhouse gases. The global warming potential (GWP) of SF_5CF_3 is currently estimated at 18,500 times that of CO_2 [5,6], greater than almost any other molecule. The stratospheric profile that was measured by Sturges et al. suggests this compound is long-lived in the atmosphere. Kennedy and Mayhew [7] have recently speculated that, because the compound is not broken down by UV photodissociation, and there are no known atmospheric sinks, ion–molecule reactions and electron attachment reactions must play a significant role in the atmospheric chemistry of SF_5CF_3. Previous reports on the electron attachment rate to SF_5CF_3 place an upper limit of approximately 1000 years on the compound's atmospheric lifetime [7–10]. In addition to its atmospheric relevance, electron attachment studies to SF_5CF_3 are of interest because of the comparisons we can make with SF_6, a molecule used in many technological applications [11,12], and with the similar molecule SF_5Cl for which we recently reported a comprehensive set of partial cross-sections for anion formation [13].

* Corresponding author at: Fachbereich Physik, Technische Universität Kaiserslautern, P.O. Box 3049, D-67653 Kaiserslautern, Germany.
E-mail address: hotop@physik.uni-kl.de (H. Hotop).

1387-3806/$ – see front matter © 2008 Elsevier B.V. All rights reserved.
doi:10.1016/j.ijms.2008.05.022

The findings of Sturges et al. [1] initiated several other studies, including IR spectroscopy [14,15], swarm experiments on electron attachment [7,8,16], and electron beam measurements of the partial cross-sections for anion formation [17,18]. The latter two studies – following pioneering work on the total attachment cross-section for this molecule by Chen et al. [19] – agreed in the observation that the dominant anion at low energies is SF_5^- while the respective findings for other anions were contradictory. Sailer et al. [17] reported a band for CF_3^- formation with a peak cross-section of 0.35×10^{-20} m^2 at 1.2 eV and a band for F^- production peaking at about 0.9 eV (cross-section 0.08×10^{-20} m^2) (in addition a weaker maximum at near-zero energies was seen in the F^- yield). Balog et al. [18] investigated low-energy electron collisions with free SF_5CF_3 molecules and with SF_5CF_3 in homogeneous clusters and in nanofilms. Like Sailer et al., they reported anion yield functions for the fragments SF_5^-, F^-, and CF_3^- with relative maximum yields of 1000, 4, and 0.03 while the Innsbruck experiment [17] gave respective maximum yields of 1000, 0.7, and 4. The Berlin measurement for F^- production [18] showed a broad band peaking at about 0.5 eV and a substantially weaker and rather wide band around 3.2 eV; their results for CF_3^- formation indicate the presence of a rather narrow peak near zero energy and a broad band around 3.5 eV.

In the present work, we combine the results from two different beam experiments to determine the partial and the total absolute cross-sections for dissociative electron attachment (DEA) to SF_5CF_3 over the energy range 0.001–12 eV. At energies below 1 eV, the SF_5^- anion is the dominant product, and we measure its DEA cross-section by two versions of the laser photoelectron attachment (LPA) method (LPA and extended laser photoelectron attachment (EXLPA), see Section 2.1) over the range 0.001–1.66 eV with energy widths of 2 meV (LPA) and about 25 meV (EXLPA). The LPA data are put on an absolute cross-section scale with reference to the well-known thermal (T = 300 K) DEA rate coefficient. The other experiment uses a pulsed electron source from a trochoidal electron monochromator with moderate resolution and a time-of-flight mass spectrometer. It yields simultaneously measured relative cross-sections for the relevant product anions with little mass and kinetic energy discrimination over the range 0.2–12 eV. The two sets of cross-section data are combined and thus yield the partial and total cross-sections for anion formation.

The paper is organized as follows: in Section 2, we describe the two experimental setups. In Section 3, we summarize some of the relevant structural and energetic properties of SF_5CF_3 and its anion, and we describe briefly the R-matrix method used to calculate the energy dependence of the DEA cross-section at low energies (<1 eV). In Section 4, we report the partial and total cross-sections and compare with the calculated cross-section and with the previous experimental results [17–19]. In addition, we calculate the dependence of the DEA rate coefficient on electron temperature for a Maxwellian electron gas at the fixed gas temperature T_G = 300 K and compare with a previous drift tube experiment [7]. We conclude with a brief summary.

2. Experimental

2.1. Laser photoelectron attachment experiment (Kaiserslautern)

In order to measure highly resolved cross-sections for anion formation in low-energy electron collisions with SF_5CF_3, we used two variants of the laser photoelectron attachment method, as discussed elsewhere in detail [20–22]. The energy range 1–200 meV was covered at resolutions of about 2 meV by the standard LPA method [20]: energy-variable photoelectrons (typical current 40 pA) are created in the reaction region with the target gas by resonant two-color photoionization of ground state potassium atoms via the excited K($4p_{3/2}$) level [21]. Higher electron energies were accessed by the extended laser photoelectron attachment method [22]: here near-zero energy photoelectrons are produced in an auxiliary photoionization chamber (distance from reaction centre about 5 cm), accelerated by a weak electric field in a guiding magnetic field (0.002 T), brought to the energy of interest prior to traversal through the target region, and subsequently accelerated and deflected onto a collector plate. Care was taken to align the exciting and the focused ionizing laser (diameter 0.12 mm) to avoid any collisions of the electron beam with surfaces on its way from the photoionization chamber to the collector since these would yield spurious low-energy electrons and thus lead to unwanted attachment processes. This is especially critical in energy ranges where the attachment cross-section is small. In this way, the drop of the SF_6^- cross-section, for example, could be followed over five orders of magnitude towards higher electron energies [22]. The effective resolution in the EXLPA experiment was about 25 meV.

Both the LPA and the EXLPA experiment were pulsed at a rate of 100 kHz: following each photoelectron production and attachment period, the infrared laser (767 nm), exciting the K(4s–$4p_{3/2}$) transition, was switched off by an acousto-optical modulator, and a voltage pulse was initiated to extract the anions. A stack of electrodes imaged the anions onto the entrance hole of a quadrupole mass filter which mass selected the species of interest. The transmitted anions were detected by a channel electron multiplier (Fa. Sjuts, background 0.02 s^{-1}).

A diffuse low-density target of SF_5CF_3 molecules (Apollo Scientific, Ltd., stated purity 99%) at the gas temperature T_G = 300 K was used without further purification. An anion mass spectrum taken at very low electron energies (using electron transfer from highly excited $K^{**}(nd)$ Rydberg atoms with $n \approx 140$; see, e.g., [21]) yielded SF_5^- as the dominant anion product. SF_6^- anions were detected at a relative intensity level of about 3.5% and attributed to a minor SF_6 impurity (relative density about 1%); correspondingly, SF_5^- anions resulting from DEA to SF_6 contribute to the SF_5^- yield at a negligible level (see Ref. [22] for the energy dependent cross-section for SF_5^- formation from SF_6). Other anions in the mass spectrum had intensities $\leq 10^{-4}$ relative to that for SF_5^-.

The LPA/EXLPA experiment provides a highly resolved yield $Y(E)$ for anion formation. This yield is proportional to the absolute DEA cross-section, i.e., $\sigma(E) = NY(E)$ where N is a normalization factor, assumed to be independent of electron energy E. The size of the normalization factor is established with reference to a known thermal DEA rate coefficient for the same process. The thermal rate coefficient $k = \langle v_{rel}\sigma(v_{rel})\rangle$, ($v_{rel}$ = relative collision velocity of the electron–molecule system) is given by the average:

$$k(T_e, T_G) = (2/m)^{1/2} \int E^{1/2}\sigma_{tot}(E; T_G) f(E; T_e)\, dE \quad (1)$$

Here, T_G denotes the rovibrational temperature of the target gas, T_e the electron temperature and $f(E;T_e)$ the electron distribution function. Note that the velocity of the gas molecules at T_G = 300 K is much smaller than the electron velocity even at electron energies as low as 0.1 meV, and the relative collision velocity v_{rel} can be replaced by the electron velocity. In calculating the rate coefficient, we use a Maxwellian distribution function which is given by

$$f(E; T_e) = 2\left(\frac{E}{\pi}\right)^{1/2} \beta^{-3/2} \exp\left(-\frac{E}{\beta}\right) \quad (2)$$

with $\beta = k_B T_e$ (k_B = Boltzmann constant). The usual thermal average in Eq. (1) requires $T_e = T_G$. In the calibration of the absolute DEA cross-section scale, we have used the thermal rate coefficient $k(T)$ measured for $T = T_e = T_G$ = 300 K.

2.2. Trochoidal electron monochromator time-of-flight (TEM–TOF) experiment (Belfast)

The DEA experiments at Belfast used a trochoidal electron monochromator in combination with a time-of-flight mass spectrometer. The apparatus has been described before in some detail [23], and only the essentials are summarized here. The electron beam path is immersed in a parallel guiding magnetic field of 0.008 T. A deflection plate in the beam-monitoring Faraday cup moves the electrons off-axis and thus prevents return of the electrons to the interaction region. The electron energy was set by floating the electron gun potentials relative to the interaction region. A plate near the filament is pulsed to send short (duration about 1 μs) pulses of electrons through the interaction region. After the electrons have left the interaction region, a repeller plate is pulsed to push the product anions from the source region. Ions pass into the acceleration region of the TOF mass spectrometer where they are further accelerated before they pass through the field-free drift region and strike the multichannel plate detector. The repetition rate of this pulse scheme is 12 kHz. The apparatus is operated under conditions where at most one ion is detected per 10 cycles to minimize any paralysis of the detector due to the arrival of two ions at the same time. The electron energy resolution (full width at half maximum) was estimated from the width of the apparent SF_6^- yield due to electron attachment to SF_6 at near-zero energies and amounted to 0.25–0.37 eV.

The experiment was carried out at room temperature (T_G = 300 K. The gas pressure in the interaction region was varied between about 5×10^{-6} and 5×10^{-5} mbar, which corresponds to number densities in the 10^{11} molecules cm^{-3} range. Spectra were measured at different pressures so that any collisional second order processes could be identified; all signals were found to be linear with pressure and no evidence for collisional effects was found. The target gas SF_5CF_3 was provided by Fluorochem Ltd. and used without further purification. From the mass spectra, taken near zero electron energy, we conclude that the maximum concentration of any SF_6 impurity was 0.2%.

3. Basic molecular information and R-matrix calculations

3.1. Structural and energetical aspects of anion formation in electron attachment to SF_5CF_3

In Fig. 1 we present simplified potential energy curves for $SF_5 + CF_3$ and $SF_5^- + CF_3$, relevant for the dominant fragmentation channel in DEA to SF_5CF_3 at low energies. Parameters for these potential curves (see Section 3.2) were obtained from G3(MP2) calculations, which represent an improvement over earlier G2(MP2) ones [8]. The G3(MP2) compound method of Curtiss et al. [24], which approximates a quantum configuration interaction (QCISD(T)) calculation with a large basis set, was used as implemented in the Gaussian-03W program [25]. An important quantity for DEA to SF_5CF_3 is its dissociation energy into the fragments $SF_5 + CF_3$; photon-induced fluorescence studies by Ruiz et al. [26] recently yielded an upper limit estimate of 3.9(3) eV. The G3(MP2) value is 3.12 eV and compatible with the upper limit. The calculations give the dissociation energy of the anion to the fragments $SF_5^- + CF_3$ as 0.26 eV (0 K) and the adiabatic electron affinity (EA) for SF_5CF_3 as 1.37 eV. Moreover, they provide the value EA(SF_5) = 4.07 eV, which places the asymptote of $SF_5^- + CF_3$ 1.11 eV below the vibrational ground state of SF_5CF_3. Recent information on the dynamics and energetics of anion formation from electron attachment to SF_6 suggested that SF_5^- formation is endothermic by 0.41 eV [27]; combining this value with the dissociation energy $D(SF_5 - F)$ = 4.35(10) eV due to Tsang and Herron [28] yields EA(SF_5) = 3.94 eV. SF_5^- formation from SF_5CF_3 is thus an exothermic process with a Q value of about 1 eV. In contrast, CF_3^- formation is an endothermic process. Using EA(CF_3) = 1.82(5) eV [29] and the G3(MP2) value for $D_0(SF_5–CF_3)$ (see above), the endothermicity for CF_3^- formation is estimated to be 1.3 eV. Likewise, F^- formation from SF_5CF_3 is an endothermic process. The G3(MP2) calculations give $D_0(F–SF_4CF_3)$ = 4.45 eV for the weakest F bond (an equatorial S–F bond), comparable to that for SF_6. With the known value EA(F) = 3.401 eV [30], one obtains an endothermicity of about 1 eV for F^- formation from SF_5CF_3. Molecular geometries, energies, and frequencies are available on the journal's website as supplementary information.

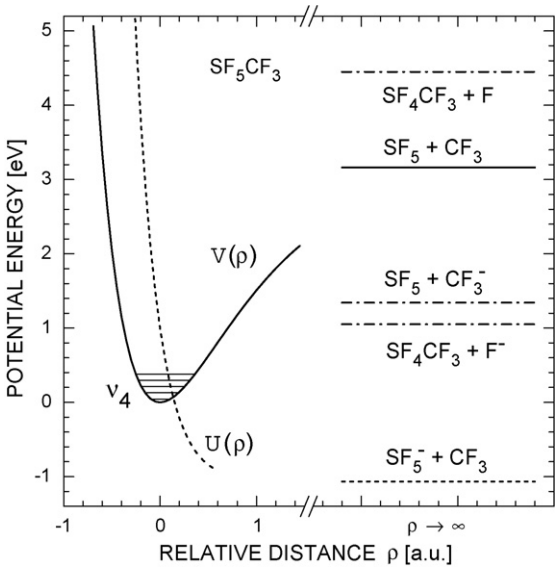

Fig. 1. Simplified potential energy curves for SF_5CF_3 and its anion. Note that the relative distance scale represents different normal coordinates depending on the symmetries and dissociation limits.

For DEA calculations (see Section 3.2) it is necessary to identify the vibrational mode of SF_5CF_3, corresponding most closely to the $SF_5–CF_3$ reaction coordinate. The first vibrational mode analysis, based on the measured infrared spectrum for SF_5CF_3, was performed by Eggers et al. [31]. They assumed that the barrier for the internal rotation of the CF_3 group is low and accordingly classified vibrational modes in terms of the C_{4V} symmetry representations. They identified the modes corresponding to internal vibrations in CF_3 (type I), modes corresponding to internal vibrations in SF_5 (type II), and the modes corresponding to the motion of SF_5 relative to CF_3 (type III).

The strongest modes of type I are $\nu_1(a_1)$, $\nu_{11}(e)$, and $\nu_3(a_1)$, of type II $\nu_2(a_1)$, $\nu_4(a_1)$, and $\nu_5(a_1)$. They observed two modes of type III, $\nu_{16}(e)$ and $\nu_{17}(e)$, but could not identify the S–C stretch mode $\nu_6(a_1)$ which is of most interest to us. By comparing the spectrum of SF_5CF_3 with those of C_2F_6 and S_2F_{10} they estimated the frequency of ν_6 as 300 cm^{-1}. This agrees rather well with the result of present MP2(FC)/6-31G(d) calculations which give the frequency of this mode as 316 cm^{-1}.

There are several more recent measurements [1,5,14,15] of the infrared spectrum of SF_5CF_3. Nielsen et al. [14] as well as Rinsland et al. [15] detected, but did not discuss a rather weak absorption band around 690 cm^{-1} which can be attributed to what Eggers et al. identified as the $\nu_4(a_1) = 1$ excitation (692 cm^{-1} = 85.8 meV) [31]. In a recent theoretical paper Li et al. [32] treated the electronic structure of SF_5CF_3 by the DFT method and performed a vibrational frequency analysis. They concluded that the barrier for the torsional

motion is low (about 1.5×10^{-4} a.u.) and therefore the CF_3 group is predicted to rotate freely at room temperature. This justifies the C_{4V} symmetry assumption employed by Eggers et al. [31]. On the other hand, Li et al. [32] present only seven vibrational frequencies and do not classify them in terms of symmetry species. Interestingly, they identify the frequency 746 cm^{-1} as corresponding to the S–C stretch. Since DFT calculations tend to overestimate frequencies, the true values may be more like 690 cm^{-1}, rather close to the spectroscopy frequency of the $\nu_4(a_1)$ mode. As will be discussed below, the LPA experiment exhibits a distinct Wigner cusp at the onset for excitation of one quantum of the $\nu_4(a_1)$ vibration, indicating that this mode is important for the primary electron attachment process.

Although for definite conclusions about the mechanism for electron attachment to SF_5CF_3 an analysis of the multidimensional potential energy anion surface is necessary, the cusp at the threshold for $\Delta\nu_4 = 1$ vibrational excitation allows us to assume that, similar to the process of electron attachment to SF_6, the electron capture initially drives the symmetric S–F stretch vibrational mode ν_4, and then due to the process of intramolecular vibrational energy redistribution (IVR), the excess energy is channeled into the S–C stretch which eventually leads to the dissociation into the fragments SF_5^- and CF_3. We will assume that the anion state is stabilized rapidly, before the IVR process becomes operative, and therefore the attachment process can be treated in a one-dimensional approximation, assuming coupling of the anion state with only the ν_4 mode. This approach is similar to our effective-range-theory treatment of electron attachment to SF_6 [33].

3.2. R-matrix calculations of the DEA cross-section for SF_5^- formation

With the aim to provide some insight into the electron attachment process we have carried out semiempirical R-matrix calculations of the DEA cross-sections. In accord with our assumption about the dominance of the ν_4 mode at the electron capture stage, we represent the neutral molecule by an effective one-dimensional potential energy curve generating the correct quantum of the ν_4 vibration, $\omega(\nu_4) = 85.8$ meV. Vibrational frequencies were calculated using the Hartree-Fock, density functional theory, and MP2. We use the corresponding reduced mass ($M = 17.353$ u) for the ν_4 motion but adopt, however, the experimental value of the ν_4 frequency. Since the asymptotic value of the neutral energy along the ν_4 coordinate is not relevant to the DEA process under consideration, we have chosen, rather arbitrarily, for the dissociation energy its value along the S–C reaction coordinate, 3.09 eV. This choice is not consistent, of course, with the one-dimensional model. We should emphasize, however, that in the present case only the coupling of the anion state with the first few vibrational states of the ν_4 mode is important for the DEA dynamics. Additional calculations using different dissociation energies, but the same vibrational frequency yielded practically the same results. Using the input data described above, we parameterize the neutral curve in the Morse form:

$$V(\rho) = A[\exp(-a\rho) - 1]^2 \tag{3}$$

where $\rho = R - R_e$ is the normal ν_4 coordinate relative to the equilibrium separation R_e, $A = 3.13$ eV and $a = 1.1853\, a_0^{-1}$ (a_0 = Bohr radius = 52.9 pm). The anion curve is parameterized in the form:

$$U(\rho) = B\exp(-2b\rho) - C\exp(-b\rho) + D \tag{4}$$

The asymptotic value of the anion curve D was obtained from the calculated [8] adiabatic electron affinity of SF_5CF_3, 1.235 eV and the dissociation energy of the anion, 0.26 eV, resulting in $D = -0.975$ eV. All other parameters were considered as empirical.

The R-matrix surface amplitude $\gamma(\rho)$ which determines the resonance width [34,35] was parameterized in the form:

$$\gamma(\rho) = \frac{\gamma_0}{\exp(\zeta\rho) + \eta} \tag{5}$$

where γ_0, ζ and η are fit parameters. Typically, $\gamma(\rho)$ is a slowly varying function, and its value between the equilibrium separation ($\rho = 0$) and the crossing point between the neutral and the anion potential curves determines the absolute magnitude of the DEA cross-section. The parameters employed in our calculations are $b = 1.972\, a_0^{-1}$, $B = 2.57$ eV, $C = 0.60$ eV, $\gamma_0 = 0.222$ $(a_0 \times \text{Hartree})^{1/2}$ (1 Hartree = 27.211 eV), $\zeta = 2.330\, a_0^{-1}$, and $\eta = 0.1725$. The vibrational motion for the calculation of the DEA cross-sections was included using the quasi-classical approximation of the R-matrix theory [35,36]. To couple the resonant anion state with the electron continuum, we calculate the electron wave functions in electron scattering channels. For these calculations we have employed the dipole moment of SF_5CF_3, $\mu = 0.384$ D [37] and the polarizability $\alpha = 8.5 \times 10^{-30}\ m^3$, as estimated by us.

4. Results and discussion

4.1. Highly resolved absolute cross-section for SF_5^- formation

In agreement with the earlier work [17,18], both the LPA and the TEM–TOF experiments confirmed that SF_5^- is by far the dominant anion formed in low-energy electron attachment to SF_5CF_3. In the following we discuss the highly resolved LPA and EXLPA results which were measured for SF_5^- over the range 0.001–1.66 eV. With reference to the thermal rate coefficient of Mayhew et al. ($k(300\,K) = 8.0(3) \times 10^{-8}\ cm^3\ s^{-1}$) [16], a reliable absolute scale was established for this partial DEA cross-section which is subsequently used to establish absolute cross-sections also for the other fragment anion channels and for total anion production.

In Fig. 2, we present the absolute DEA cross-section for SF_5^- formation from SF_5CF_3 determined in this work by combining the LPA (0.001–0.19 eV) and the EXLPA (0.19–1.66 eV) data. The energy resolution was about 2 meV for the LPA data and about 25 meV for the EXLPA results, respectively. The LPA anion yield was averaged over six original data points (about 6 channels per meV) and interpolated with respect to an integer meV scale; the EXLPA anion yield was measured with a channel width of 1 meV and normalized to the LPA data in the energy range from 160 to 190 meV where the LPA and EXLPA yields exhibited identical slopes. Below about 0.5 eV the partial SF_5^- cross-section is identical with the total cross-section since other fragment ions do not contribute at a significant level (see below); therefore, it is possible to use the *total* thermal rate coefficient $k(T = 300\,K)$ to establish the absolute cross-section scale shown in Fig. 2.

Close to $E = 86$ meV, a clear downward-step like Wigner cusp is observed (see especially the expanded view in Fig. 2b) which is attributed to the interaction of the primary attachment process with the channel for vibrational excitation of the $\nu_4(a_1)$ mode. As is known from the previous high-resolution work on molecules such as SF_6 [20,22], CCl_4 [38], CF_3Br [39], and CF_3I [40], these Wigner cusps are characteristic for the vibrational modes which are active in the attachment process. Note that for SF_5^- formation, the vibrational modes which may be considered to promote dissociation of the primary anion complex $(SF_5CF_3)^-$ towards the fragments $SF_5^- + CF_3$ are not identical with the channel interaction mode $\nu_4(a_1)$ which basically represents a symmetric internal vibration of the SF_5 group.

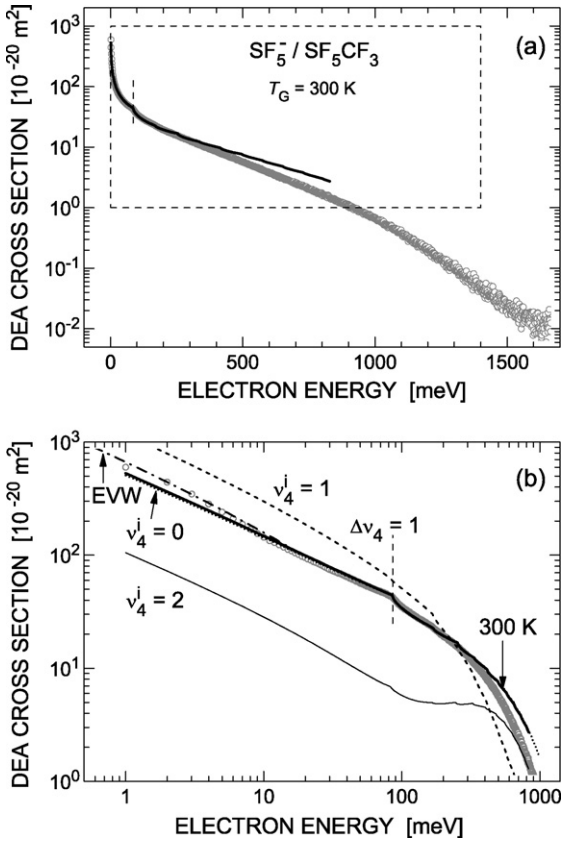

Fig. 2. Absolute cross-section for SF_5^- formation due to electron attachment to SF_5CF_3 (gas temperature T_G = 300 K). (a) Combined LPA/EXLPA data (open gray circles) over the range 0.001–1.66 eV, compared with the R-matrix cross-section (full curve) for energies up to 0.83 eV. Close to E = 86 meV, the measured and calculated cross-sections exhibit downward step-like structure (see also (b)) due to the interaction between the attachment and the $\Delta\nu_4 = 1$ vibrational excitation channel. (b) Closer view at the low-energy region (0.5–500 meV, indicated in (a) by broken lines). The chain curve shows the extended Vogt-Wannier (EVW) cross-section, adjusted in absolute value to the experimental cross-section at E = 2 meV. The dotted, short-dash and full thin curves represent the calculated state-specific DEA cross-sections for the initial vibrational levels $\nu_4^i = 0$, 1, and 2, respectively. For further details, see text.

The observation of the cusp structure at the $\Delta\nu_4(a_1) = 1$ vibrational onset was incorporated into our theoretical model, discussed in Section 3.2, whose results are also included in Fig. 2a and b (full curves). Good agreement between the experimental and the calculated cross-sections – including the shape of the cusp structure at the $\Delta\nu_4 = 1$ threshold – is observed at energies up to about 0.25 eV. The calculations also predict weaker cusps at the higher $\Delta\nu_4 \geq 2$ onsets, but these features are not apparent in the measurements. Towards higher energies the calculated cross-section progressively stays above the experimental values by up to a factor two. These deviations can be removed by a different choice of the surface amplitude $\gamma(\rho)$ which, however, varies rather fast with ρ. We think that this reflects, in an empirical way, the complexity of the actual multidimensional surface dynamics of the DEA process.

We note that the calculated DEA cross-sections (full curves in Fig. 2a and b) represent the vibrational average with regard to the initial thermal population of the $\nu_4(a_1)$ mode. Since the ν_4 quantum (85.8 meV [31]) is about three times larger than k_BT, most of the population (≈96%) resides in the initial $\nu_4^i = 0$ ground state. The state-specific DEA cross-section for $\nu_4^i = 1$ actually exceeds the $\nu_4^i = 0$ cross-section for E < 0.23 eV (by more than a factor of two below E = 16 meV) as a result of a more favourable Franck-Condon factor for the transition from the neutral to the anion state; the $\nu_4^i = 1$ population thus leads to a non-negligible, but small contribution to the vibrationally averaged DEA cross-section. The cross-section for $\nu_4^i = 2$ is smaller (by about a factor of three at low energies) than that for $\nu_4^i = 0$, and its contribution to the thermal average is negligible.

At low electron energies, we compare the measured cross-section *shape* with the prediction of the extended Vogt-Wannier (EVW) capture model [41,42] (chain curve in Fig. 2b). In these calculations, we use the spectroscopic electric dipole moment of 0.384 D [37] and the estimated polarizability 8.5×10^{-30} m^3. The predicted EVW cross-section is about a factor of three higher than the measured absolute DEA cross-section, indicating – in contrast to, e.g., the cases of SF_6 or CCl_4 [41,42] – that for the molecule SF_5CF_3 the efficiency for anion formation only amounts to about one third of the electron capture events. In the R-matrix description of the DEA process, the EVW cross-section behaviour is built into the theory via the long-range electron-molecule interactions. The lowering of the DEA cross-section from the EVW value is due to two effects: (i) non-optimal Franck-Condon factors for the transition from the neutral molecule to the initial temporary negative ion (TNI) state upon electron capture; (ii) a smaller than unity survival probability for the evolution of the TNI to the dissociated pair $SF_5^- + CF_3$. This evolution involves IVR and thus coupling to the motion which leads to dissociation of the TNI. The processes involved in (ii) will in general depend on the initial thermal energy in the various participating vibrational modes, and this dependence can lead to the Arrhenius-type rise in the thermal ($T \equiv T_e = T_G$) rate coefficient $k(T)$ (activation energy 0.025 eV), observed by Miller et al. [8] over the temperature range 295–563 K. We note that the R-matrix calculations described above yield a very weak dependence of $k(T)$ on T (variation less than 3% over the mentioned temperature range). This deviation from the experimental observations [8] is attributed to the one-dimensional approximation employed in the calculations which does not incorporate IVR and dissociation. This issue was recently discussed in some detail for DEA to CF_3Br [39].

Over the energy range 0.2–0.9 eV (see Fig. 2a), the energy dependence of the cross-section for SF_5^- formation is well described by a simple exponential decrease $\sigma(E; SF_5^-) \propto \exp(-E/a)$ with a = 0.246 eV. At higher energies, the decrease becomes more rapid as a result of the competing decay of the primary anion complex into F^- anions. At about E = 1.25 eV the partial cross-section for F^- formation (see Section 4.2) becomes equal to that for SF_5^- production. Following a minimum at about 2 eV, the SF_5^- yield exhibits a rather broad, near-bell-shaped band towards higher energies with a maximum at 3.6 eV. We attribute this higher lying band (which also produces F^- anions with almost the same probability, see Section 4.2) to the dissociation of the first excited anion resonance which is of a repulsive nature.

In Fig. 3 we compare the yields for SF_5^- formation from three different experiments over the energy range 0–4 eV. In the two diagrams (a) and (b), the full circles (gray) represent the combined LPA/EXLPA anion yield, taken from Fig. 2. In Fig. 3a we compare with the SF_5^- yield measured with the Belfast TEM–TOF apparatus (open circles). From these data we constructed a joint cross-section for SF_5^- formation by combining the LPA/EXLPA cross-section with the Belfast data for $E \geq 2.2$ eV through a brief interpolation (broken curve) from 1.6–2.2 eV. This interpolation and the resolution of the Belfast data were chosen in such a way that the convolution of the joint cross-section with a Gaussian resolution function of 370 meV (FWMH) resulted in a close reproduction (full curve) of the Belfast data over the full energy range. We note that the energy scale of the Belfast data was adjusted so as to match optimally that of the convoluted spectrum. Note that the rather low resolution of the

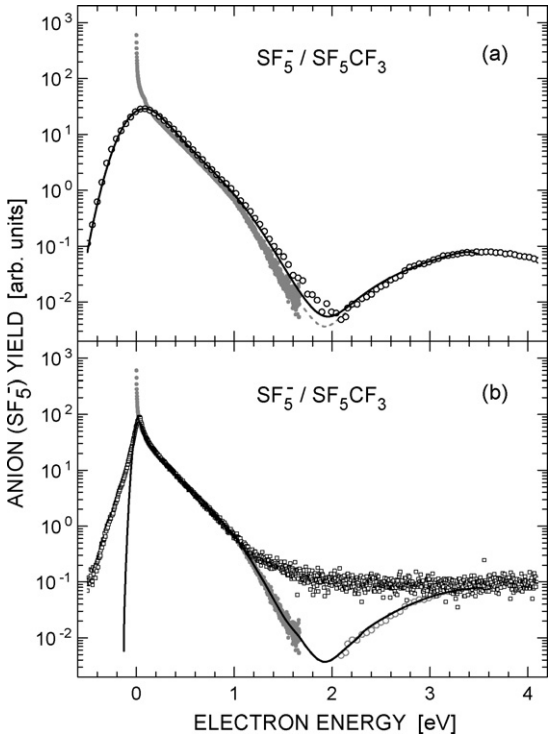

Fig. 3. Comparison of the highly resolved LPA/EXLPA yield for SF_5^- formation with (a) the TEM-TOF results (Belfast), and (b) the TEM-QMS results (Innsbruck [17]). For details see text.

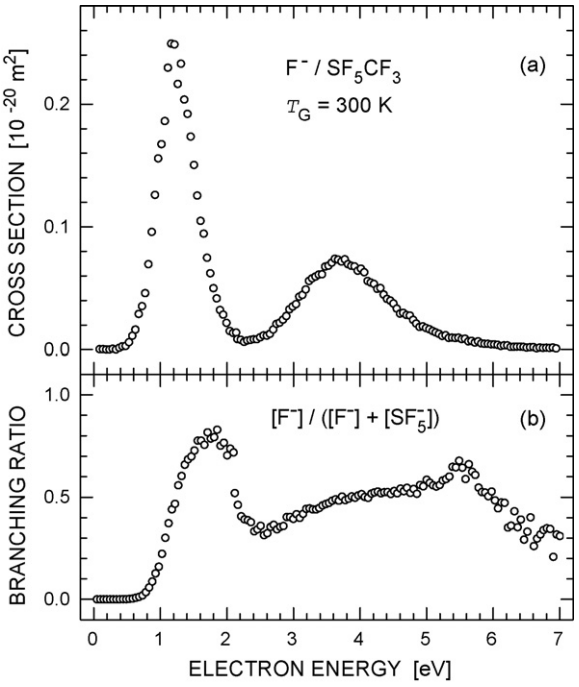

Fig. 4. (a) Absolute cross-section for F^- formation due to electron attachment to SF_5CF_3 ($T_G \approx 300$ K) and (b) anion branching ratio $R(E) = \sigma(F^-)/[\sigma(F^-) + \sigma(SF_5^-)]$, both over the energy range 0–7 eV.

Belfast experiment introduces substantial deviations of the measured anion yield function from the true DEA cross-section only in energy ranges where sharp features are present, notably at very low energies.

In Fig. 3b, we compare the SF_5^- anion yield reported by the Innsbruck group [17] (open squares, quoted resolution 80 meV) with the yield (full curve), obtained by convolution of our joint cross-section with a Gaussian of 80 meV (FWHM). The energy scale of the Innsbruck data was adjusted such as to optimally match that of the convoluted spectrum. Over the range 0.1–1 eV, good agreement is observed between the two absolute cross-sections (the absolute scale of the Innsbruck cross-section was established with reference to the total cross-section reported by Chen et al. [19]; the latter work will be discussed below in connection with Fig. 6). At near-zero energies the Innsbruck yield surpasses the convoluted spectrum by about 20%. This observation may be explained by the effects of an increased electron path at the lowest energies, due to helical motion and/or multiple traversals through the attachment region. At the higher energies, the Innsbruck data stay above the LPA/EXLPA cross-section as well as above that measured in Belfast. They do not show the second maximum for SF_5^- formation, clearly observed in the Belfast experiment around 3.6 eV. It appears that the Innsbruck data have a lower dynamical range than the other two data sets; possibly, they are influenced towards higher nominal energies by contributions from low-energy electrons which may be produced, e.g., by scattering from orifices. In our EXLPA work, we found it very important to align the electron source carefully and thus avoid any collisions of the accelerated and decelerated electrons with any of the collimating, potential-defining orifices. Finally, we note that the SF_5^- yield measured at Berlin [18] is in qualitative agreement with the Innsbruck data, but has less statistical quality; it also misses the second peak around 3.6 eV.

4.2. Absolute cross-section for F^- formation

In Fig. 4a, we present the absolute partial cross-section for F^- formation over the range 0–7 eV. The energy calibration of this spectrum is fixed with reference to the simultaneously taken SF_5^- spectrum for which the energy scale is derived from that of the LPA/EXLPA spectrum (Fig. 3a). At energies above about 0.4 eV, the F^- yield surpasses the noise level, exhibits a first maximum at $E = 1.2$ eV with a cross-section $\sigma(E = 1.2\text{ eV}; F^-) \approx 0.25 \times 10^{-20}$ m^2 which is followed by a minimum around 2.3 eV and a second maximum located at about 3.7 eV with a cross-section of 0.07×10^{-20} m^2. As explained in section 3.1, F^- formation from SF_5CF_3 is an endothermic process. From the energy for the resolution-corrected threshold in Fig. 4a (estimated as 0.6 eV), and assuming that this threshold is shifted to lower energies from the true onset by the average rovibrational energy in the SF_5CF_3 molecule at 300 K (0.21 eV), one obtains an estimate of 4.2 eV for the separation energy of F from SF_5CF_3.

The first maximum in the F^- yield, located at 1.2 eV, is attributed to the combination of two effects: (i) the primary attachment process occurs via the lowest-lying anion resonance which is also responsible for SF_5^- formation at low energies; (ii) dissociation of this primary negative ion state to the energetically accessible channels, yielding SF_5^- and F^- anions, proceeds with a characteristic energy-dependent branching ratio $R(E) = \sigma(F^-)/[\sigma(F^-) + \sigma(SF_5^-)]$, reflecting the channel-specific fragmentation probabilities $p(F^-)$ and $p(SF_5^-)$. These probabilities depend on the total energy of the primary anion and on the asymptotic energies of the respective dissociated fragment pairs. They may be obtained from unimolecular decay theory (including the energy-dependent autodetachment process), see the recent work by Troe et al. on the energy dependent branching ratio $SF_5^-/(SF_5^- + SF_6^-)$ resulting from electron attachment to SF_6 [27].

In Fig. 4b we present the energy-dependent branching ratio $R(E)$ over the range 0–7 eV. From 0.6 to 1.8 eV (i.e., within the

first anion resonance) the ratio monotonically rises from zero to a maximum value of 80%. Towards higher energies, the second anion resonance first starts to influence and then dominates the branching ratio which attains an average value of about 0.5 in the range around the center of the second anion resonance (3.6 eV).

In Fig. 4a, we did not compare with the results reported previously for F^- formation [17,18]. These earlier data show some clear deviations from our results. The Innsbruck group reported a broad band for F^- production peaking at about 0.9 eV with a peak cross-section of 0.08×10^{-20} m^2 which presumably corresponds to the band which we observe to peak at 1.2 eV with a maximum cross-section of 0.25×10^{-20} m^2. In addition, a weaker maximum at near-zero energies was observed (Fig. 3 in Ref. [17]); this peak must be due to secondary reactions, as discussed, e.g., in DEA work on C_2Cl_4 by the Innsbruck group [43]. The Berlin group [18] reported a rather broad band for F^- production, peaking at about 0.5 eV and a substantially weaker and wide band around 3.2 eV. For unclear reasons, these two bands are shifted to lower energies by about 0.7 and 0.5 eV, respectively, relative to those observed in the present work.

4.3. Absolute cross-sections for formation of the anions CF_3^-, SF_4^-, and SF_3^-

In Fig. 5, we summarize the absolute partial cross-sections for the five notable fragment anions, as observed in DEA to SF_5CF_3 over the energy range 0–12 eV. In both the SF_5^- and the F^- channel, a weak band is found around 11 eV in addition to those observed around 3.6 eV and below 2 eV. The anions CF_3^-, SF_4^-, and SF_3^- are formed with small cross-sections (below 3×10^{-23} m^2).

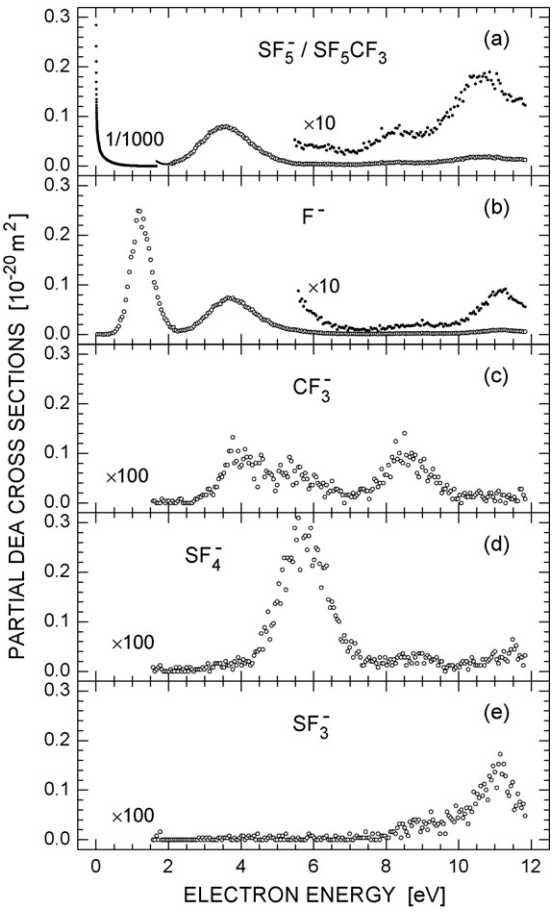

Fig. 5. Partial absolute cross-sections for DEA to SF_5CF_3 (E = 0–12 eV), yielding the fragment anions: (a) SF_5^-, (b) F^-, (c) CF_3^-, (d) SF_4^-, and (e) SF_3^-.

The Belfast cross-section for CF_3^- formation has a first rise above the noise level at about 2.7 eV and exhibits two broad bands with maxima at about 4 eV and 8.5 eV. The earlier results for the anion CF_3^- deviate substantially from the present cross-section and must have been influenced by systematic errors. The CF_3^- data, reported by Sailer et al. [17] over the range 0–3 eV, show a single broad band with a first rise near 0.4 eV and a maximum at about 1.1 eV. This finding is in conflict with the estimated endothermicity for CF_3^- formation from SF_5CF_3 (1.3 eV, see Section 3.1). We note that the Innsbruck data for SF_5CF_3 were taken in the presence of the calibrant gas CCl_4 [17].[1] The anion Cl_2^- (with a mass close to that of CF_3^-) is a fragment resulting from DEA to CCl_4 and exhibits a DEA band with a very similar appearance and energy location as compared to that reported for CF_3^- by Sailer et al. (Fig. 2 in Ref. [17]). We therefore suggest that the CF_3^- band reported in [17] was in fact due to Cl_2^- formation from CCl_4. The CF_3^- data, reported by Balog et al. [18] over the range 0–4.7 eV, exhibit a rather narrow peak at 0 eV and a broad band with a maximum at about 3.5 eV. The latter band appears to correspond to our band peaking around 4 eV. The peak at near-zero energy in the CF_3^- yield must have been caused by an experimental artefact (probably by secondary reactions).

DEA cross-sections for the weak fragment anions SF_4^- (Fig. 5d) and SF_3^- (Fig. 5e) are reported here for the first time. SF_4^- formation is characterized by a clear band centered at about 5.7 eV. SF_3^- production becomes noticeable at energies above about 8 eV and shows a maximum at about 11.1 eV, i.e., 1.7 eV below the adiabatic ionization energy of SF_5CF_3 [44].

Using the absolute cross-sections shown in Fig. 5, we determined energy-integrated cross-sections for the five anions over the respective characteristic bands and in this way obtained band-specific branching ratios. In Table 1 we list the energy location of the maximum of the respective band, the measured FWMH of the band, the integration range, the integrated cross-section (in 10^{-20} m^2 eV), and the branching ratio in two different forms, namely as the ratio of the integrated cross-sections and as the ratio of the band maxima, both normalized to 100% for the second band of SF_5^- (integration window 2.09–6.99 eV). The branching ratios of the band *integrals* should be independent of the experimental resolution, see the integrals in Table 1 for the original LPA data (0.001–2.09 eV) and for the LPA data convoluted with Gaussian resolution functions of 80 and 370 meV, respectively. The band integrals are thus especially suitable for comparison with other work. The integral of the Belfast data for the first SF_5^- band is found to be in close agreement with the integral of the LPA data; in part, this agreement reflects the fact that the Belfast data were matched to the convoluted LPA cross-section at higher energies. The integral of the Innsbruck data is 14.6% larger than that of the LPA data; part of this difference is due to the fact that the Innsbruck cross-section exceeds the convoluted LPA cross-section near the maximum.

In contrast, the ratios of the band maxima exhibit substantial differences whenever the experimental resolution plays a role (in the present case this is only relevant for the SF_5^- band extending down to zero energy). Thus it is not advisable to compare such a maximum intensity for a near-zero energy peak with the maximum intensity of (broader) bands at higher energies. In general, authors should quote the energy-integrated anion yield of

[1] W. Sailer, private communication.

Table 1
Energy-integrated absolute cross-sections for anion formation due to electron attachment to the molecule SF_5CF_3 (rovibrational temperature T_G = 300 K)

Anion	Peak position (eV)	Peak maximum ($\times10^{-20}$ m^2)	Peak width (FWHM) (eV)	Branching ratio (max.) ($\times100$)	Integration range (eV)	Integral ($\times10^{-20}$ m^2 eV)	Branching ratio (integral) ($\times100$)
SF_5^-	"Zero energy"						
LPA[a]	0.001	600	–	–	0.001–2.09	15.51	11,931
ΔE_{80}[b]	0.025	73.8	0.13	95,359	−0.13–2.09	15.51	11,931
Innsbr.[c]	0.004	89.2	0.10	115,250	−0.50–2.09	17.78	13,677
ΔE_{370}[d]	0.082	28.8	0.46	37,209	−0.50–2.09	15.51	11,931
Belfast[e]	0.082	28.8	0.47	37,209	−0.89–2.09	15.65	12,043
SF_5^-[f]	3.53	0.0774	1.61	100.00	2.09–6.99	0.1300	100.00
	8.31	0.0056	≈1.1	7.24	7.19–9.04	0.0071	5.44
	10.71	0.0167	≈2.1	21.58	9.04–11.83	0.0324	24.93
F^-[f]	1.19	0.2493	0.64	322.14	0.38–2.26	0.1734	133.39
	3.70	0.0732	1.47	94.59	2.26–6.99	0.1236	95.11
	≈9	0.0019	–	2.44	7.58–9.53	0.0033	2.56
	11.19	0.0090	≈1.5	11.64	9.53–11.23	0.0124	9.52
CF_3^-[f]	4.01	0.00105	≈1.1	1.35	2.69–4.75	0.00123	0.95
	5.38	0.00072	≈1.5	0.94	4.75–6.99	0.00096	0.74
	8.56	0.00101	≈1.5	1.30	6.99–10.02	0.00156	1.20
SF_4^-[f]	5.67	0.00289	≈1.5	3.74	3.57–7.33	0.00447	3.44
	8.75	0.00036	–	0.47	7.33–9.58	0.00051	0.39
	11.44	0.00052	–	0.68	9.58–11.83	0.00050	0.39
SF_3^-[f]	≈9	0.00040	–	0.52	7.33–9.58	0.00046	0.36
	11.1	0.00153	≈1.3	1.97	9.58–11.83	0.00190	1.46

[a] Peak position and maximum are given for E = 1 meV (the cross-section is divergent for $E \to 0$).
[b] LPA cross-section convoluted with Gaussian energy resolution function of FWHM = 80 meV (see Fig. 3b).
[c] Data of the Innsbruck group [17] (see Fig. 3b).
[d] LPA cross-section convoluted with Gaussian energy resolution function of FWHM = 370 meV (see Fig. 3a).
[e] Data of the Belfast experiment (see Fig. 3a).
[f] Data of the Belfast experiment (see Fig. 5).

observed DEA bands, but we consider it mandatory that energy-integrated (absolute or relative) cross-sections are provided for narrow, resolution-limited bands, especially for the band extending down to zero energy.

We emphasize that maximum intensities for near-zero energy peaks, measured with decelerated electron beams (with or without a magnetic guiding field) are often questionable for various reasons. In the absence of a guiding magnetic field, it is nearly impossible to reach near-zero kinetic energies in a controlled way. In the presence of a guiding magnetic field, transverse velocity components prevent the range close to zero kinetic energy being accessed; moreover, electron spiralling effects introduce uncertainties in the path length and thus in the anion yield. Even if transverse components are ruled out or reduced (as in the EXLPA experiment in which the photoelectrons are formed with zero kinetic energy), there is still the uncertainty whether the electrons are decelerated to near-zero energy in the proper reaction volume and whether the electrons traverse this volume only once. In our opinion, the only trustworthy, presently available approach to reliably measure the shape of DEA cross-sections at energies below about 50 meV is the laser photoelectron attachment experiment in which monoenergetic electrons with variable kinetic energy undergo attachment reactions in essentially the same (nearly) field-free volume in which they are formed by photoionization.

4.4. Total DEA cross-section and the dependence of the DEA rate coefficient on electron temperature

Summation of the five partial absolute DEA cross-sections in Fig. 5 yields the total absolute DEA cross-section $\sigma_{tot}(E)$ for SF_5CF_3, shown as the full curve in Fig. 6. For comparison, we included the partial cross-sections for SF_5^- (open circles) and F^- formation (open squares), and the sum cross-section for the formation of CF_3^-, SF_4^-, and SF_3^- (full diamonds). Note that these data were obtained at the fixed gas temperature T_G = 300 K.

In Fig. 6, we also included the total cross-section for anion production (open triangles), reported by Chen et al. for a target gas temperature $T_G \approx 300$ K (see Fig. 2 in Ref. [19]). These authors used a magnetically guided electron beam (monochromatized to an effective energy width of about 80 meV by the retarding-potential-difference method) and measured the total anion current formed.

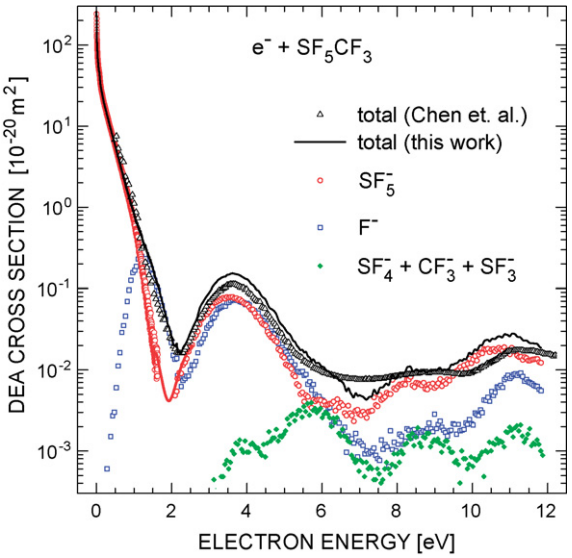

Fig. 6. Total and partial absolute cross-sections for anion formation in electron-SF_5CF_3 collisions (gas temperature T_G = 300 K). Total cross-section, full curve (present work) and open triangles (Chen et al. [19]); SF_5^-, open circles; F^-, open squares; sum of CF_3^-, SF_4^-, and SF_3^-, full diamonds.

The electron energy and the cross-section for SF_5CF_3 were placed on absolute scales, respectively, with reference to measurements with the target molecule N_2O, using the absolute attachment cross-section for N_2O obtained by Rapp and Briglia [45]. Very good overall agreement is observed between the total cross-section reported by Chen et al. [19] and that obtained in the present work by a different method, both with regard to the absolute size of the cross-sections and the energy locations of the main bands. We note that the Chen et al. data shown in Fig. 6 were obtained by digitizing the results in their Fig. 2; in view of the 0.08 eV resolution and the steepness of the plot near zero energy we did not include data points at energies below 0.5 eV. At energies above 6.5 eV, where the total cross-section stays below 3×10^{-22} m^2, the two sets of cross-sections differ from each other by no more than a factor of two.

In the following, we discuss the dependence of the total DEA rate coefficient $k(T_e; T_G)$ on electron temperature T_e for the fixed gas temperature $T_G = 300$ K. We calculate $k(T_e; T_G)$ with (1), using the total DEA cross-section in Fig. 6 and a Maxwellian electron distribution function. The latter choice appears well justified for the recent drift-tube experiment of Mayhew et al. [16] in which CO_2 was used as the carrier gas at atmospheric pressure and room temperature ($T_e = T_G = 300$ K). Carbon dioxide is known to rapidly establish Maxwellian equilibrium for the electron distribution function. In the earlier measurements of Kennedy and Mayhew [7] in which the mean electron energy $\langle E \rangle$ was varied from 0.04 to 1.9 eV, the carrier gas N_2 was used for $\langle E \rangle$ <0.5 eV, and Ar for $\langle E \rangle$ >0.5 eV.

In Fig. 7, we compare the rate coefficient $k(T_e; T_G = 300\,\text{K})$, calculated with the new total absolute DEA cross-section over the range $T_e = 50$–$20{,}000$ K (i.e., mean electron energy $\langle E \rangle = (3/2)k_B T_e = 0.0065$–$2.6$ eV), with the temperature dependence reported by Kennedy and Mayhew [7]. Good overall agreement between the two data sets is observed over the broad temperature range covered in the experiment. Note that for the buffer gases N_2 and Ar the electron distribution function in this drift tube experiment will deviate from the Maxwellian form assumed in the calculations. The relatively small differences between the measured and calculated rate coefficients will therefore in part be due to deviations of the experimental electron distribution function from the Maxwellian form. The calculated rate coefficient $k(T_e; T_G = 300\,\text{K})$ is identically recovered up to electron temperatures $T_e = 800$ K ($\langle E \rangle = 0.103$ eV) when the partial DEA cross-section for SF_5^- formation is used instead of the total cross-section. At $T_e = 12000$ K ($\langle E \rangle = 1.551$ eV), the rate coefficient for SF_5^- formation still amounts to 95% of the total rate coefficient.

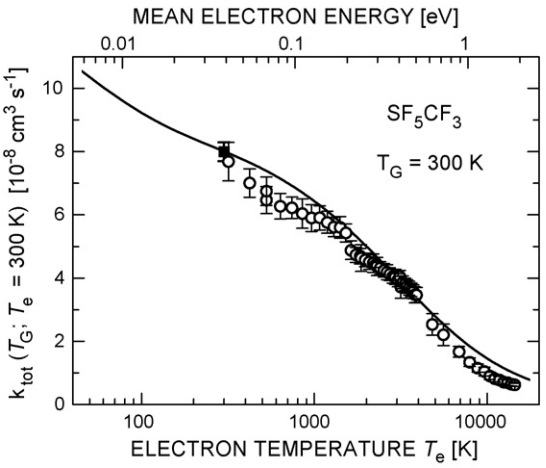

Fig. 7. Dependence of the total rate coefficient for DEA to SF_5CF_3 on electron temperature T_e over the range of 50–20,000 K at the fixed gas temperature $T_G = 300$ K.

5. Conclusions

Partial and total absolute cross-sections for dissociative electron attachment to the molecule trifluoromethyl sulfurpentafluoride (SF_5CF_3) at the gas temperature $T_G = 300$ K are reported over a broad range of electron energies ($E = 0.001$–12 eV). The absolute scale for the cross-sections is determined with reference to the thermal ($T = 300$ K) rate coefficient for anion formation ($8.0(3) \times 10^{-8}$ cm^3 s^{-1}).

Below 1 eV, SF_5^- is the dominant product anion and formed through the lowest anion state which cuts the neutral SF_5CF_3 potential close to the S–C equilibrium distance. The highly resolved laser photoelectron attachment data exhibit a downward Wigner cusp at 86 meV, indicating that the $\nu_4(a_1)$ vibrational mode is important for the primary attachment dynamics. Semiempirical R-matrix calculations of the energy dependent cross-section for SF_5^- formation yield good agreement with the experimental DEA cross-section, but cannot reproduce the activation energy for the thermal DEA rate coefficient observed in a swarm experiment.

Both SF_5^- and F^- anions are formed with similar yields through the first excited resonance located near 3.6 eV. Towards larger electron energies, the anions CF_3^-, SF_4^-, ands SF_3^- anions are produced in addition with low cross-sections. Summation of the partial (mass-resolved) cross-sections yielded a total absolute cross-section for anion formation over the energy range 0.001–12 eV; the only previously reported total attachment cross-section for SF_5CF_3 ($T_G \approx 300$ K), obtained with a different method by Chen et al. [19] at a resolution of about 80 meV, is found to be in good agreement with our results. Our highly resolved DEA cross-section is used to calculate the dependence of the rate coefficient for dissociative electron attachment over a broad range of electron temperatures for the fixed gas temperature $T_G = 300$ K; good agreement is observed between the calculated values and those obtained in a drift tube experiment.

G3(MP2) calculations were carried out to provide information on the reaction energetics. Molecular geometries and energies are available through the journal as a Supplementary file.

Acknowledgements

This cooperative work has been stimulated by the ESF Network EIPAM (electron induced processing at the molecular level). The work at Kaiserslautern has been supported by the Deutsche Forschungsgemeinschaft (HO 427/29) and by the Research Center OTLAP. K.G. would like to thank the European Social Fund for providing a PhD studentship. T.A.F., K.G. and L.M.G. would like to thank the EPSRC for their support of this work through grant EP/F031025/1. C.A.M. gratefully acknowledges support from ESF (EIPAM) and the EPSRC funded UK Nonthermal Plasma Network for travel grants to the Technische Universität Kaiserslautern and Queen's University Belfast, respectively, and EPSRC. I.I.F. was supported by the US National Science Foundation, Grant PHY-0652866. T.M.M. acknowledges support from the U.S. Air Force Office of Scientific Research. We thank W. Sailer and R. Balog for providing their DEA data in numerical form. One of us (H.H.) gratefully acknowledges helpful correspondence and discussions with W. Sailer.

Appendix A. Supplementary data

Supplementary data associated with this article can be found, in the online version, at doi:10.1016/j.ijms.2008.05.022.

References

[1] W.T. Sturges, T.J. Wallington, M.D. Hurley, K.P. Shine, K. Sihra, A. Engel, D.E. Oram, S.A. Penkett, R. Mulvaney, C.A.M. Brenninkmeijer, Science 289 (2000) 611.
[2] L. Huang, L. Zhu, X. Pan, J. Zhang, B. Ouyang, H. Hou, Atmos. Environ. 39 (2005) 1641.
[3] W.-T. Tsai, J. Fluorine Chem. 128 (2007) 1345.
[4] W.-T. Tsai, J. Hazard. Mater. 149 (2007) 747.
[5] P.A. Kendall, N.J. Mason, G.A. Buchanan, G. Marston, P. Tegeder, A. Dawes, S. Eden, P. Limão-Vieira, D.A. Newnham, Chem. Phys. 287 (2003) 137.
[6] P. Limão-Vieira, S. Eden, P.A. Kendall, N.J. Mason, A. Giuliani, J. Heinesch, M.-J. Hubin-Franskin, J. Delwiche, S.V. Hoffmann, Int. J. Mass Spectrom. 233 (2004) 335.
[7] R.A. Kennedy, C.A. Mayhew, Int. J. Mass Spectrom. 206 (2001) i–iv.
[8] T.M. Miller, S.T. Arnold, A.A. Viggiano, W.B. Knighton, J. Chem. Phys. 116 (2002) 6021.
[9] T. Takahashi, T. Nakayama, Y. Matsumi, S. Solomon, T. Gejo, E. Shigemasa, T.J. Wallington, Geophys. Res. Lett. 29 (2002) 7/1.
[10] R.Y.L. Chim, R.A. Kennedy, R.P. Tuckett, Chem. Phys. Lett. 369 (2003) 697.
[11] L.G. Christophorou, J.K. Olthoff, J. Phys. Chem. Ref. Data 29 (2000) 267.
[12] L.G. Christophorou, J.K. Olthoff, Fundamental Electron Interactions with Plasma Processing Gases, Kluwer Academic/Plenum Publ., New York, 2004.
[13] M. Braun, M.-W. Ruf, H. Hotop, P. Cicman, P. Scheier, T.D. Märk, E. Illenberger, R.P. Tuckett, C.A. Mayhew, Int. J. Mass Spectrom. 252 (2006) 234.
[14] O.J. Nielsen, F.M. Nicolaisen, C. Bacher, M.D. Hurley, T.J. Wallington, K.P. Shine, Atmos. Environ. 36 (2001) 1237.
[15] C.P. Rinsland, S.W. Sharpe, R.L. Sams, J. Quant. Spectrosc. Radiat. Transfer 82 (2003) 483.
[16] C.A. Mayhew, A.D.J. Critchley, D.C. Howse, V. Mikhailov, M.A. Parkes, Eur. Phys. J. D 35 (2005) 307.
[17] W. Sailer, H. Drexel, A. Pelc, V. Grill, N.J. Mason, E. Illenberger, J.D. Skalny, T. Mikoviny, P. Scheier, T.D. Märk, Chem. Phys. Lett. 351 (2002) 71.
[18] R. Balog, M. Stano, P. Limao-Vieira, C. König, I. Bald, N.J. Mason, E. Illenberger, J. Chem. Phys. 119 (2003) 10396.
[19] C.L. Chen, R.E. Wootton, P.J. Chantry, Proceedings of the Seventh International Conference on Gas Discharges and their Applications, London, England (Peregrinus, London), 1982, p. 321.
[20] D. Klar, M.-W. Ruf, H. Hotop, Aust. J. Phys. 45 (1992) 263.
[21] J.M. Weber, E. Leber, M.-W. Ruf, H. Hotop, Eur. Phys. J. D 7 (1999) 587.
[22] M. Braun, S. Barsotti, S. Marienfeld, E. Leber, J.M. Weber, M.-W. Ruf, H. Hotop, Eur. Phys. J. D 35 (2005) 177.
[23] T.A. Field, A.E. Slattery, D.J. Adams, D.D. Morrison, J. Phys. B 38 (2005) 255.
[24] L.A. Curtiss, P.C. Redfern, K. Raghavachari, V. Rassolov, J.A. Pople, J. Chem. Phys. 110 (1999) 4703.
[25] M.J. Frisch, G.W. Trucks, H.B. Schlegel, G.E. Scuseria, M.A. Robb, J.R. Cheeseman, J.A. Montgomery Jr., T. Vreven, K.N. Kudin, J.C. Burant, J.M. Millam, S.S. Iyengar, J. Tomasi, V. Barone, B. Mennucci, M. Cossi, G. Scalmani, N. Rega, G.A. Petersson, H. Nakatsuji, M. Hada, M. Ehara, K. Toyota, R. Fukuda, J. Hasegawa, M. Ishida, T. Nakajima, Y. Honda, O. Kitao, H. Nakai, M. Klene, X. Li, J.E. Knox, H.P. Hratchian, J.B. Cross, V. Bakken, C. Adamo, J. Jaramillo, R. Gomperts, R.E. Stratmann, O. Yazyev, A.J. Austin, R. Cammi, C. Pomelli, J.W. Ochterski, P.Y. Ayala, K. Morokuma, G.A. Voth, P. Salvador, J.J. Dannenberg, V.G. Zakrzewski, S. Dapprich, A.D. Daniels, M.C. Strain, O. Farkas, D.K. Malick, A.D. Rabuck, K. Raghavachari, J.B. Foresman, J.V. Ortiz, Q. Cui, A.G. Baboul, S. Clifford, J. Cioslowski, B.B. Stefanov, G. Liu, A. Liashenko, P. Piskorz, I. Komaromi, R.L. Martin, D.J. Fox, T. Keith, M.A. Al-Laham, C.Y. Peng, A. Nanayakkara, M. Challacombe, P.M.W. Gill, B. Johnson, W. Chen, M.W. Wong, C. Gonzalez, J.A. Pople, Gaussian 03 Revision C. 02, Gaussian, Inc., Wallingford, CT, 2004.
[26] J.A. Ruiz, A. Kivimäki, M. Stankiewicz, E.M. Garcia, M. Coreno, S. Ali, J. Koperski, E. Rachlew, G.V. i Serrano, V. Feyer, R. Tuckett, Phys. Chem. Chem. Phys. 8 (2006) 5199.
[27] J. Troe, T.M. Miller, A.V. Viggiano, J. Chem. Phys. 127 (2007) 244304.
[28] W. Tsang, J.T. Herron, J. Chem. Phys. 96 (1992) 4272.
[29] H.-J. Deyerl, L.S. Alconcel, R.E. Continetti, J. Phys. Chem. A 105 (2001) 552.
[30] C. Blondel, C. Delsart, F. Goldfarb, J. Phys. B 34 (2001) L281.
[31] D.F. Eggers Jr., H.E. Wright, D.W. Robinson, J. Chem. Phys. 35 (1961) 1045.
[32] Z. Li, J. Yang, J.G. Hou, Q. Zhu, Chem. Phys. Lett. 359 (2002) 321.
[33] I.I. Fabrikant, H. Hotop, M. Allan, Phys. Rev. A 71 (2005) 022712.
[34] A.M. Lane, R.G. Thomas, Rev. Mod. Phys. 30 (1958) 257.
[35] I.I. Fabrikant, Phys. Rev. A 43 (1991) 3478.
[36] S.A. Kalin, A.K. Kazansky, J. Phys. B 23 (1990) 4377.
[37] M.S. Malmberg, A.A. Maryott, J. Chem. Phys. 53 (1970) 1614.
[38] D. Klar, M.-W. Ruf, H. Hotop, Int. J. Mass Spectrom. 205 (2001) 93.
[39] S. Marienfeld, T. Sunagawa, I.I. Fabrikant, M. Braun, M.-W. Ruf, H. Hotop, J. Chem. Phys. 124 (2006) 154316.
[40] S. Marienfeld, I.I. Fabrikant, M. Braun, M.-W. Ruf, H. Hotop, J. Phys. B 39 (2006) 105.
[41] I.I. Fabrikant, H. Hotop, Phys. Rev. A 63 (2001) 1, 022706.
[42] H. Hotop, M.-W. Ruf, M. Allan, I.I. Fabrikant, Adv. Atom. Mol. Opt. Phys. 49 (2003) 85.
[43] H. Drexel, W. Sailer, V. Grill, P. Scheier, E. Illenberger, T.D. Märk, J. Chem. Phys. 118 (2003) 7394.
[44] D.M.P. Holland, D.A. Shaw, I.C. Walker, I.J. McEwen, E. Aprà, M.F. Guest, J. Phys. B 38 (2005) 2047.
[45] D. Rapp, D.D. Briglia, J. Chem. Phys. 43 (1965) 1480.